Detection of Abnormal Cardiac Activity using Principal Component Analysis

Ariel Greisas, Sharon Zlochiver

Department of Biomedical Engineering, Tel Aviv University, Tel Aviv, Israel

Abstract

Electrogram-guided ablation has been recently developed for allowing better detection and localization of abnormal atrial activity that may be the source of arrhythmogeneity. Nevertheless, no clear indication for the benefit of using electrograms guided ablation over empirical ablation was established thus far, and there is a clear need of improving the localization of cardiac arrhythmogenic targets for ablation. In this work we propose a new approach for detection and localization of irregular cardiac activity during ablation procedures that is based on dimension reduction algorithms and principal component analysis (PCA). We employ mathematical modeling and computer simulations to demonstrate the feasibility of the new approach for two well established arrhythmogenic sources for irregular conduction – spiral waves and patchy fibrosis. Our results show that the PCA method can differentiate between focal ectopic activity and spiral wave activity. Moreover, the technique allows the detection of spiral wave cores. Fibrotic patches larger than 2 mm^2 could also be visualized using the PCA method, both for quiescent atrial tissue and for tissue exhibiting spiral wave activity. We envision that this method, contingent to further numerical and experimental validation studies in more complex, realistic geometrical configurations and with clinical data, can improve existing atrial ablation mapping capabilities, thus increasing success rates and optimizing arrhythmia management.

1. Introduction

ATRIAL Fibrillation (AF) is the most common sustained arrhythmia in adults, affecting millions of patients in the U.S. alone and associated with increased morbidity and mortality [1]. Consequently, atrial ablation procedure, a non-pharmacological therapy, has become an attractive alternative procedure for curing AF in symptomatic patients. In this procedure, radiofrequency (RF) energy (typically 300-1000 kHz) is delivered to cardiac tissue sustaining suspected arrhythmogenic sources causing permanent ablation, in order to prevent either arrhythmogenic impulse generation or the conduction of arrhythmias [2]. Nonetheless, due to the uncertainty regarding the exact location of the arrhythmogenic source, these repetitive empirical ablations often result in unnecessary applications of RF energy that cause inadvertent injury and thromboembolic complications in the atrial tissue. Electrogram-guided ablation techniques have been recently developed in the hope of minimizing these negative consequences [3]. Nevertheless, no clear indication for the benefit of using electrogram guided ablation over empirical ablation was established as reported empirical ablation success rates are similar and range between 60-90% for both techniques [4]. Therefore, following the limitations in the currently practiced ablation techniques, the inconsistent success rates and the ambiguities in interpreting the electrograms, there is a clear need of improving the localization of cardiac arrhythmogenic targets for ablation.

In this work we propose a new approach for automated detection and localization of irregular cardiac activity during electrogram-guided ablation procedures that is based on dimension reduction algorithms and principal component analysis (PCA). Our method produces manifolds that allow an easy visualization and detection of possible arrhythmogenic ablation targets characterized by irregular conduction. We employ mathematical modelling and computer simulations to demonstrate the feasibility of the new approach for two well established arrhythmogenic sources for irregular conduction – spiral waves and patchy fibrosis. Spiral waves, or rotors, are stable or meandering re-entrant circuits which have become widely accepted as drivers for many cardiac arrhythmias [5]. Fibrosis, the second source for irregular conduction that we tested in this study, refers to the proliferation of cardiac fibroblast and the concomitant collagenous matrix accumulation that develop during myocardial remodelling during many cardiomyopathies. Fibrotic clusters, or patches, are known to initiate and maintain arrhythmias in the cardiac tissue via various mechanisms [6], e.g., by creating microstructural obstacles that slow or block electrical pulse conduction, by reducing regional coupling or by anchoring micro-

anatomical re-entry.

2. Methods

2.1. Electrophysiological modeling

The electrical activity in the heterogeneous cardiac tissue was simulated using an extended model that incorporates both fibroblasts and myocytes, as proposed by Sachse et al. [7]. The original model accounts only for diffusive fibrosis, in which a constant ratio of fibroblasts to myocytes spans the entire tissue. In order to extend its relevance to patchy fibrosis, we have applied several modifications to facilitate spatial variations in the amount of fibroblasts coupled to a single myocyte. The extra-cellular potential, φ_e, and the myocyte and fibroblast transmembrane voltages, V_{myo} and V_{fib}, respectively (all in [mV]), are governed by the following coupled equations:

$$\nabla\left(\left(\sigma_{i\_myo}+\sigma_{i\_fib}+\sigma_e\right)\nabla\varphi_e\right)= -\nabla\left(\sigma_{i\_myo}\nabla V_{myo}\right)-\nabla\left(\sigma_{i\_fib}\nabla V_{fib}\right) \quad (1)$$

$$C_{myo}\frac{\partial V_{myo}}{\partial t}=-I_{ion_{myo}}+\left[\frac{\nabla\left(\sigma_{i_{myo}}\nabla V_{myo}\right)+\nabla\left(\sigma_{i_{myo}}\nabla\varphi_e\right)}{\beta_{myo}}\right]-G_{gap}\cdot N_{fib}\left(V_{myo}-V_{fib}\right)+I_{stim} \quad (2)$$

$$C_{fib}\frac{\partial V_{fib}}{\partial t}=-I_{ion_{fib}}+\left[\frac{\nabla\left(\sigma_{i_{fib}}\nabla V_{fib}\right)+\nabla\left(\sigma_{i_{fib}}\nabla\varphi_e\right)}{\beta_{fib}}\right]+G_{gap}\left(V_{myo}-V_{fib}\right) \quad (3)$$

where $I_{ion_{myo}}$ and $I_{ion_{fib}}$[pA] are the total myocyte and fibroblast ion channel current across the membrane, C_myo and C_fib [pF] are the myocyte and fibroblast membrane capacitance, $\sigma_{i_{myo}}$ and σ_{i_fib} [S/m] are the intracellular myocyte and fibroblast conductivity tensors due to the existence of homocellular gap junctions, σ_e [S/m] is the medium extracellular conductivity tensor, N_{fib} is the local number of fibroblasts connected to a single myocyte, G_{gap} [μS] is the gap junction conductance of a coupled fibroblast-myocyte pair, I_{stim} [pA] is an external stimulation current, and β_{myo} and β_{fib} [1/ m^3] refer to the myocyte and fibroblast per volume ratio, respectively. Equations (1)-(3) describe a tri-layer geometrical configuration, in which each volume unit consists of three parallel domains – the extracellular space, the fibroblast intracellular space and the myocyte intracellular domain. The domains are electrically coupled to each other by membrane currents (between the extracellular and intracellular spaces) and by the heterocellular gap junctions (between a myocyte and fibroblast). The human atrial myocyte ionic kinetics of Courtemanche et al. [8] were employed for calculating $I_{ion_{myo}}$, with the addition of I_{K-ACh} as in [9] with a small acetylcholine concentration of [ACh]=0.03μM in order to enable the establishment of stable spiral waves. Fibroblast membrane currents, $I_{ion_{fib}}$ were calculated using the ionic kinetics of MacCannel et al. [10]. A two-dimensional square tissue of size 25x25 mm was modelled in a bi-layer scheme, which assembles atrial myocytes in a matrix-like monolayer, along with fibroblasts that are aligned on top in a parallel matrix to simulate a fibrotic tissue, where appropriate. Fibrotic patches were modelled with sizes ranging from 1 to 14 mm^2. Within each fibrotic patch, each myocyte was coupled to the same number of fibroblasts, N_{fib}, having a maximum value of 10, while the rest of the myocytes in the tissue were not coupled to any fibroblast.

Two patterns of electrical conduction were simulated, focal activity and spiral waves. Focal activity was initiated by repetitive local point stimulations at (x,y)=(12,12) mm using pulse magnitude and duration of I_{stim}=100μA and T=1ms, respectively, and with a frequency of 12.8Hz. Spiral waves were initiated using standard S1-S2 cross-field stimulation, with S1 occupying the top 5 rows of the tissue (I_{stim}=100μA, T=1ms, width=25mm, length=1.25mm), and S2 given 110ms following S1 at the top-left quarter of the tissue (I_{stim}=100μA, T=1ms, width=12.5mm, length=12.5mm).

2.2. Principal Component Analysis

Principal Component Analysis (PCA) is a well-established technique for dimensionality reduction that is based on eigenvector multivariate analysis and transformation. To find the principal components for the measured signals, the covariance matrix of *M* - The measurement matrix, consisted of the extracellular potentials recorded for a duration of 2000ms in an array of 8x8 pseudo-electrodes, is first calculated, resulting in an 64x64 matrix C. Next, an eigenvalue decomposition is performed on the symmetric matrix C. The final step is the projection of the original data on the eigenvectors, resulting in the principal components matrix, T. To reduce the problem dimensionality, only the first two principal components (called the primary components) were considered for further analysis and visualization.

Following the PCA transformation, the primary components of each measurement signal were charted on a 2D map, and an optimal 2nd order polynomial manifold corresponding to the entire 64 measurements was fitted using minimum square error optimization. To visualize the degree of regularity in local activity we therefore

calculated the Euclidean distance of each point on the 2D primary components map (each corresponding to one measurement signal) to the manifold, and generated 2D regularity maps that represent those distances.

3. Results

3.1. PCA for the detection of focal activity and spiral waves

The PCA algorithm was applied on data measured for two types of periodic cardiac activity - focal activity and

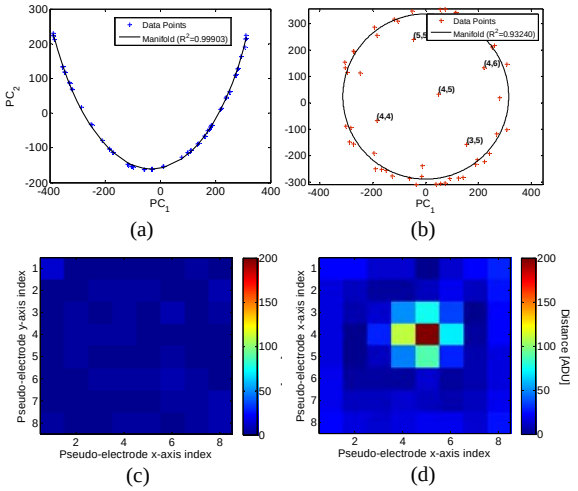

Figure 1. Typical manifolds and regularity maps for ectopic focal activity vs. spiral wave activity. (a,b) Primary components 2D charts for the two activity types. (c,d) Regularity maps for the two activity types.

spiral wave, as described in the methods section. As shown in Figures 1a and 1b, while a focal point activity resulted in an open, disconnected, manifold, the spiral wave activity yielded a closed loop, circular manifold. In addition, the focal activity manifold exhibited a high degree of regularity in its trajectory, meaning that the principal component data points of all pseudo-electrodes measurements were almost perfectly laid on the manifold curve (manifold fitting correlation coefficient of R^2=0.99). In contrast, the spiral wave manifold showed some degree of irregularity, with principal component data points scattered in the vicinity of the manifold trajectory (R^2=0.93). The regularity maps given in Figures 1c and 1d clearly visualize the high degree of regularity sustained by focal activity in comparison to spiral wave activity. Moreover, the location of the spiral wave core is easily observed due to its higher degree of irregularity. Therefore, PCA seems to effectively distinguish between the two arrhythmia mechanisms – focal activity and spiral wave.

3.2. PCA for detection of fibrotic patches

In this part of the study, we examined the feasibility of the PCA technique to address the clinical need of reliable mapping of fibrotic patches, which are an established arrhythmogenic source in diseased cardiac tissues. Two scenarios were considered, the first of which corresponds to a cardiac tissue at rest and the other is that of an existing spiral wave in the cardiac tissue.

Fibrotic patches of sizes ranging between 1 to 14 mm^2 (corresponding to areas covered by 4x4 to 15x15 cells) were added to the lower right part of the tissue, and fibroblast densities ranging from N_{fib}=0 to N_{fib}=10 were applied. Focal activity due to point stimulation was established as described in the methods section. Figure 2 presents several examples of the regularity maps established from the primary components maps that were generated for the electrode-array measurements. While the visualization of a relatively small patch occupying 3x3 grid cells and having $N_{fib} = 3$ was insufficient (top-left example), the location and size of the fibrotic patches could be easily detected in the other cases. Visualization quality improved (i.e. the electrodes over the fibrotic patch exhibited higher distance from the manifold) with either higher N_{fib} value or larger patch area.

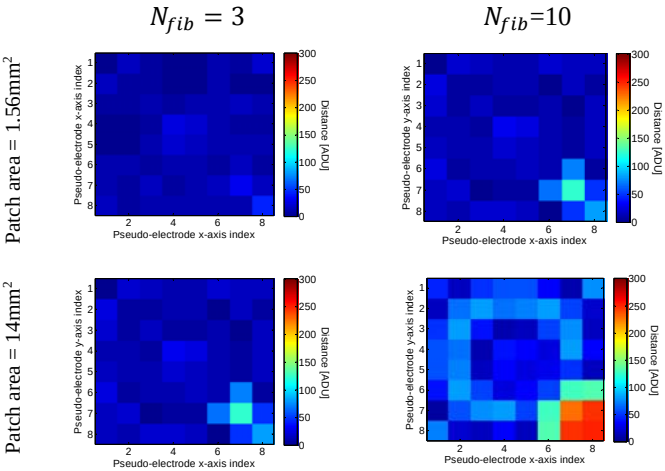

Figure 2. PCA for detection of fibrotic patches by Point stimulation applied to a quiescent tissue. Regularity maps are shown for 2 sizes of fibrotic patches – 1.56 and 14mm^2 (top and bottom rows, respectively) – and for two values of N_{fib} – 3 and 10 (left and right columns, respectively).

Figure 3a summarizes the results, and shows the regularity map values corresponding to the electrode closest to the center of the fibrotic patch for various sizes of fibrotic patches and values of N_{fib}. The figure demonstrates a generally monotonic increase in these values as both the fibrotic tissue size and N_{fib} increased. By assuming a qualitative visible distance threshold of

100 (as marked by the horizontal blue line in Figure 2), fibrotic patches of size smaller than ~2mm^2 cannot exhibit sufficiently good visualization on the regularity maps, regardless of N_{fib}. Next, we examined the feasibility of the PCA technique to detect fibrotic patches in a scenario of an existing spiral wave activity. Fibrotic patches of similar sizes and density as in the previous section were added to the lower right part of the tissue. Spiral wave activity was initiated as described in the methods section.

As was the case for the point stimulation, the detection quality in the sense of intensity and size improved with both increased fibrotic patch size and increased N_{fib}. Figure 3b summarizes the results in a similar manner as in Figure 3a. This figure also demonstrates a generally monotonic increase in these values as both the fibrotic tissue size and N_{fib}increased, with the former factor being more dominant. By setting a qualitative visible distance threshold of 100, here again fibrotic patches of size smaller than ~2mm^2 could not be sufficiently visualized on the regularity maps.

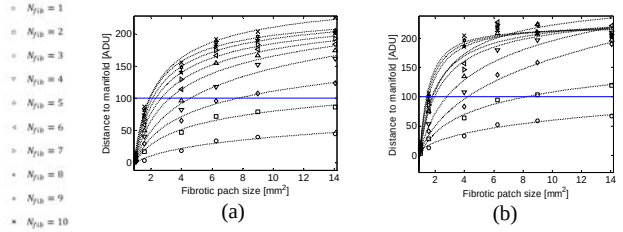

Figure 3. PCA for detection of fibrotic patches by (a) Point stimulation and (b) spiral wave.

4. Discussion

Our results show that when the PCA method was applied to simulations of two basic arrhythmia drivers – focal ectopic activity and spiral waves – two significantly different primary components maps were observed (Figure 1). Therefore, PCA may not only be employed in practical applications to distinguish between these two types of drivers and to optimize treatment, but also to detect the location of spiral wave cores.

With respect to irregularities created by fibroblast clusters, our results showed that fibrotic patches can be visualized, both in a quiescent tissue and in a tissue that sustains spiral wave activity. Detection and visualization quality improved for larger fibrotic patches and for larger fibrosis density (as determined by N_{fib}), see Figure 3, with the minimum detectable fibrotic patch size being 2mm^2.

In conclusion, this study has demonstrated the feasibility of PCA to detect and map atrial conduction abnormalities resulting from ectopic foci, spiral waves or fibrotic patches. We believe that this method, contingent to further numerical and experimental validation studies in more complex, realistic geometrical configurations and with clinical data, can improve existing atrial ablation mapping capabilities.

References

[1] Wattigney WA, Mensah GA. Croft JB.. Increased atrial fibrillation mortality: United States, 1980-1998. Am J Epidemiol 2002; 155: 819–826.

[2] Oral H. Atrial fibrillation: mechanisms, features, and management," In: D.P. Zipes and J. Jalife, editors. Cardiac Electrophysiology, from cell to bedside. 5th ed. Philadelphia, Saunders Elsevier; 2009. p. 577.

[3] Atienza F, Almendral J, Jalife J, Zlochiver S, Ploutz-Snyder R, Torrecilla EG, Arenal A, Kalifa J, Fernandez-Aviles F, Berenfeld O. Real-time dominant frequency mapping and ablation of dominant frequency sites in atrial fibrillation with left-to-right frequency gradients predicts long-term maintenance of sinus rhythm. Heart Rhythm 2009; 6:. 33-40.

[4] Lim KT, Knecht S, Wright M, Haissaguerre M. Atrial substrate ablation in atrial fibrillation. In: D.P. Zipes and J. Jalife, editors. Cardiac Electrophysiology, from cell to bedside. 5th ed. Philadelphia, Saunders Elsevier; 2009. p. 1059.

[5] Mandapati R, Skanes A, Chen J, Berenfeld O, Jalife J. Stable microreentrant sources as a mechanism of atrial fibrillation in the isolated sheep heart. Circulation 2000;.101: 194-199.

[6] Tanaka K, Zlochiver S, Vikstrom KL, Yamazaki M, Moreno J, Klos M, Zaitsev AV, Vaidyanathan R, Auerbach DS, Landas S, Guiraudon G, Jalife J, Berenfeld O, Kalifa J. Spatial distribution of fibrosis governs fibrillation wave dynamics in the posterior left atrium during heart failure. Circ Res 2007; 101: 839-847.

[7] Sachse FB, Moreno AP, Seemann G, Abildskov JA. A model of electrical conduction in cardiac tissue including fibroblasts. Ann Biomed Eng 2009;37: 874-89.

[8] Courtemanche M. Ramirez RJ, Nattel S. Ionic mechanisms underlying human atrial action potential properties: insights from a mathematical model. Am J Physiol 1998;275: H301-21.

[9] Kneller J, Zou R, Vigmond EJ, Wang Z, Leon LJ, Nattel S. Cholinergic atrial fibrillation in a computer model of a two-dimensional sheet of canine atrial cells with realistic ionic properties. Circ Res 2002;. 90: E73-87.

[10] MacCannell KA, Bazzazi H, Chilton L, Shibukawa Y,. Clark RB, Giles WR. Mathematical model of electrotonic interactions between ventricular myocytes and fibroblasts. Biophys J 2007;92:4121–4132.

Address for correspondence.

Ariel Greisas
6a Hachartzit St, Mazkeret Batya, Israel, 76804
Ariel.greisas@gmail.com